Digital Object Identifier 10.1109/TPEL.2021.3065028

IEEE Transactions on Power Electronics

Modulation for Cascaded Multilevel Converters in PV Applications with High Input Power Imbalance

Youngjong Ko

Markus Andresen

Kangan Wang

Marco Liserre

Suggested Citation

Y. Ko, M. Andresen, K. Wang and M. Liserre, "Modulation for Cascaded Multilevel Converters in PV Applications with High Input Power Imbalance," in IEEE Transactions on Power Electronics.

This article has been accepted for publication in a future issue of this journal, but has not been fully edited. Content may change prior to final publication. Citation information: DOI 10.1109/TPEL.2021.3065028, IEEE Transactions on Power Electronics

Modulation for Cascaded Multilevel Converters in PV Applications with High Input Power Imbalance

Youngjong Ko, *Member*, IEEE, Markus Andresen, *Member*, IEEE,
Kangan Wang, Marco Liserre, *Fellow*, IEEE

***Abstract*—Cascaded multilevel inverters, such as the cascaded H-Bridge (CHB) converter, are an attractive solution for multi-string photovoltaic (PV) systems, because they enable direct connection to the medium voltage grid and maximum power point tracking of multiple strings. As a challenge of the topology, the operation with high power imbalance in the strings is constrained by the over-modulation. This limitation is analyzed for sinusoidal modulation and the impact on the maximum power imbalance is demonstrated. For increasing the operating range with maximum power tracking in the strings, a discontinuous modulation with extended maximum power imbalance and reduced losses is proposed. The method is analyzed in terms of maximum power imbalance, efficiency and power quality. In addition, the method is validated on an experimental test bench.**

***Index Terms*—Cascaded H-Bridge (CHB), photovoltaic (PV), multi-string architecture, module mismatch, power imbalance, discontinuous modulation**

I. Introduction

The increasing power rating of grid-connected photovoltaic (PV) systems has resulted in the proposal of multi-string systems [1], [2]. In such systems, a mismatch in the operating conditions, such as partial shading, unequal ambient temperatures and inconsistent module characteristics is commonly found [3], leading to the unbalanced power generation among phases and strings and consequently, a reduced utilization of PV modules. The power imbalance issue can be addressed on the phase level [4], [5] or the string level with individual power point trackers [6].

The Cascaded H-Bridge (CHB) inverters are an attractive solution for the multi-string PV systems as shown in Fig. 1, which allow individual connection of each string to isolated DC buses [3], [7]. Therefore, this topology enables maximum power point tracking of the different strings. Hence, different maximum power of the PV modules under mismatched operating conditions can be harvested. In this context, the maximum power imbalance among cells poses a challenge to the operation under heavy mismatched condition.

The solution to handle the power imbalance among cells has been discussed in literature and can be categorized into two solutions, which differ by the modulation: level-shifted carriers and phase-shifted carriers [8]. The level-shifted carriers based solution technically aims at modifying the rotating sequence of carriers [9], [10]. This solution features a good dynamic response and higher capability for power imbalance compared to the phase-shifted carrier based solution. However, the phase-shifted carrier modulation is typically preferred with various advantages. One of the critical advantages is the higher equivalent switching frequency, which allows a superior power quality, lower filter requirement or higher efficiency through reduced switching frequency [11]. As a solution based on the phase-shifted carriers, a PI controller was proposed in [12], which modifies the modulation index of each cell to independently control the transferred power of the H-bridges. Furthermore, in [13], several PI based solution are discussed and different solution are compared in terms of the design procedure and the influence on system performance. On the other hand, since the phase-shifted carrier solution is based on the modified modulation index, it is straight forward that the over-modulation is a limiting factor of the power imbalance capability. In other word, the modulation index of a higher loading cell is increasing, which causes the over-modulation under the heavy mismatched condition. This impacts the power quality and may affect the closed-loop control to become unstable [10], [14], [15].

In order to ensure the stable operation under heavy mismatched conditions, several advanced control strategies were proposed [14]–[18]. A mixed staircase-PWM technique in the

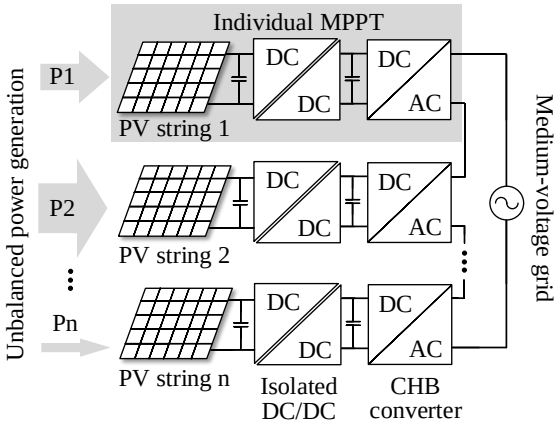

Fig. 1: Multi-string architecture with individual MPPT for each string, causing unbalanced power generation.

Y. Ko is with the Department of Electrical Engineering and Industry 4.0 Convergence Bionics Engineering, Pukyong National University, Busan 48513, South Korea (yjko@pknu.ac.kr).

K. Wang is with Logistics Engineering College, Shanghai Maritime University, Shanghai, China (kangan_wang@163.com).

M. Andresen and M. Liserre are with the Chair of Power Electronics, Christian-Albrechts-University of Kiel, Kiel 24143, Germany ({ma, ml}@tf.uni-kiel.de).

CHB PV systems, where one cell operates in PWM mode while the others are kept in either 'charging' or 'discharging' to decrease the switching frequency and increase power extraction [14]–[16]; A novel power equalization method based on the combination of mixed staircase-PWM technique and different zero-sequence injection methods is proposed in [17], which can deal with inter-bridge power imbalance and inter-phase power imbalance at the same time. Reference [18] shows the third harmonic compensation of the non-reserved cells and reserved cell. The negative third harmonic component is injected into the reserved cell to keep the peak value of its combined modulation waveform being unity. Reactive power compensation strategy was discussed to extend the operation region by optimizing the reactive power distribution among H-bridge cells in [19], [20]. A compensation strategy combining reactive power compensation with improved LS-PWM method is proposed to extend the operating range in terms of heavy module mismatch, which further reduces the switching events and minimizes the required amount of reactive power [20]. However, even though the optimized reactive power compensation algorithm was adopted, there still is uncertainty about the reactive power injection or absorption without any request from a grid operator. In this concern, this work is motivated to investigate a method, which aims to extend the power imbalance capability, and consequently in order to ensure the stability under heavy mismatched condition.

This work proposes a discontinuous modulation strategy, which operates with the phase-shifted carriers. The proposed method has two variants of modulation signal, clamped for additional power and non-clamped for reduced power, and the power imbalance is handled by manipulating clamping angle. In fact, this principle was first proposed in [21], in order to address the reliability of modular smart transformer. Its major objective is to perform the power routing, which implies the redistribution of the total power in purpose depending on their remaining useful lifetime. On the contrary to this, this work aims at considering the power imbalanced inevitably caused by different power generation from each PV string. Hence, the total power shall be varied depending on the generation of each PV panel, which represents a challenge in implementation of the discontinuous method. In order to implement the discontinuous modulation strategy for a high number of CHB cells, a grouping strategy is proposed. A analytical demonstration of the potential is shown and validated with simulations and experimental results. Finally, it is noted that this work considers the two-stage structure shown in Fig. 1, which implies that the DC-link voltage of all cells is regulated at a same level. Hence, the following analysis is performed, assuming the identical DC-link voltages. On the other hand, the single-stage system (consisting of PV strings and CHB without DC/DC stage) has been employed for the large-scale PV application. In this structure, the identical DC-link voltages are not guaranteed due to different maximum power points of the strings. Therefore, the impact of the different voltages must be considered, even though the principle proposed in this work can be still applied.

This work is structured as following. In section II, the module mismatch issue in the multi-string architecture is introduced, arriving at a conclusion that over-modulation of CHB inverter is a critical limiting factor for power imbalance capability. The principle of the proposed discontinuous modulation is introduced, together with proposing generalized implementation strategy in section III. Then, the power imbalance capability and the influence on efficiency and power quality are analyzed in section IV. Before finalizing this work in section VI, the proposed method is validated in the developed test bench in section V.

II. Power imbalance in the H-Bridges

CHB converters have been proposed early for PV applications, where the power imbalance among the cells represents a challenge for the operation of the converter [3], [22]. In the operation with unequal power and voltage processed by each of the CHB cells, the total harmonic distortion is affected. For optimizing the THD in the presence of unbalanced operation conditions, a generalized harmonic control has been proposed, which minimizes the THD in these conditions [23]. Discontinuous modulation was proposed for regulating thermal stress for the components in the different building blocks and for processing different power in the different cells [2], [3] and even generalization to an arbitrary number of cells has been proposed [24].

Considering the multi-string architecture shown in Fig. 1, the operating point of each string is depending on multiple factors like the number of connected PV panels, the irradiance on the panels and the MPPT algorithm. Particularly, a mismatch in the irradiance causes different maximum power points and therefore a power imbalance among the strings. In this context, the solution can be addressed in modulation of the CHB inverter. Assuming that the CHB inverter is modulated with the conventional sinusoidal modulation, the modulation index is controlled depending on the power. This results in a higher modulation index for higher power. In this context, the modulation index could be increased over the linear operation region under heavy power imbalance. The converter operation in the non-linear region would cause a DC-link voltage drift, and in turn, power quality is significantly decreased. Hence, the power imbalance capability is limited by the linear modulation region. Furthermore, the limited capability can be translated into a limited capability of the maximum power point tracking, leading to loss of the maximum power generation.

A single phase CHB inverter is shown in Fig. 2, which consists of n cells. In order to evaluate the maximum power imbalance, the modulation index for each cell M_j needs to be considered, which is obtained by [25]:

$$M_j = \frac{V_j}{V_{dc,j}}. \tag{1}$$

Here, V_j represents the amplitude of j^{th} cell output voltage and $V_{dc,j}$ are the j^{th} DC-link voltage (where $j = 1,2,..,n$ and n is the total number of cells). In the following analysis, the unity power factor is considered. Furthermore, it is assumed that the DC-link voltage of each cell is equal to V_{dc}, i.e. $V_{dc,1} = V_{dc,2} = .. = V_{dc,n} = V_{dc}$. On the other hand, the nominal modulation index of the whole inverter M_n can be expressed by the ratio

This article has been accepted for publication in a future issue of this journal, but has not been fully edited. Content may change prior to final publication. Citation information: DOI 10.1109/TPEL.2021.3065028, IEEE Transactions on Power Electronics

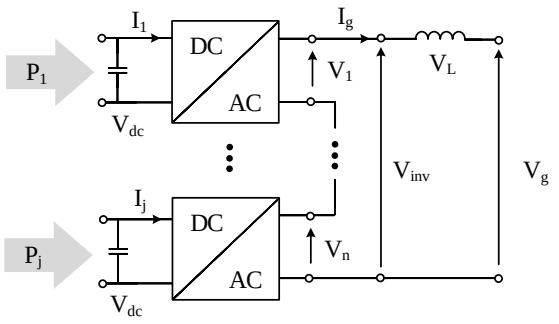

Fig. 2: Simplified structure of CHB inverter, consisting of n cells.

between the total DC-link voltage nV_{dc} and the amplitude of the grid voltage V_g as

$$M_n = \frac{V_g}{nV_{dc}} = \frac{\sum_{j=1}^{n} M_j}{n}. \tag{2}$$

Also, the nominal modulation index is equal to the average value of the summation of all cells' modulation index, assuming that the voltage drop across the inductor V_L is neglected.

On the other hand, as shown in (1), the cell modulation index determines a respective cell output voltage, modifying its power. The cell output power P_j is calculated as

$$P_j = \frac{1}{2} V_j I_g = V_{dc} I_j \tag{3}$$

where I_j is the DC current of j^{th} cell and I_g is the amplitude of grid current. As it can be seen, the cell power is solely dependent on the cell output voltage, since the grid current is equally shared by all series connected cells. Moreover, assuming that the power losses of CHB inverter is zero, the cell input power $V_{dc}I_j$ is identical with the cell output power.

The total power of the whole inverter P is obtained by a summation of cell power as shown in

$$P = \sum_{j=1}^{n} P_j = \frac{1}{2} V_g I_g. \tag{4}$$

In order to derive a relation between the cell modulation index and the cell power, rearranged (1) and (4) are substituted in (3). The result is shown in

$$M_j = \frac{V_g}{V_{dc}} \frac{P_j}{P}. \tag{5}$$

From (5), it is clear that the cell modulation index is proportional to the respective cell power (i.e. $M_j \propto P_j$). As mentioned before, the over-modulation is the major limiting factor to the power imbalance capability. This implies that the maximum modulation index decides the capability.

The degree of power imbalance ε is defined by a ratio between the average power of total power and the cell power as the left equation in (6) [8]. By substituting (2) and (5) into (6), it can be expressed by the modulation index like right equation.

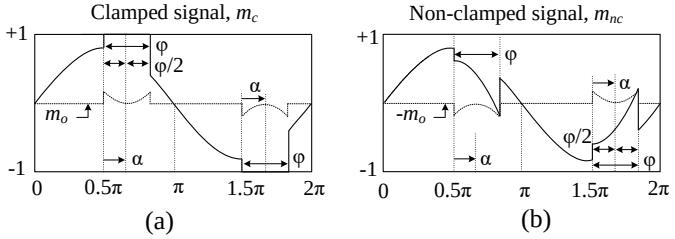

Fig. 3: Proposed discontinuous modulation for power imbalance: (a) for additional power (ε>1) and (b) for reduced power (ε<1).

$$\varepsilon = \frac{P_j}{\frac{1}{n}P} = \frac{M_j}{M_n}. \tag{6}$$

Consequently, the maximum power imbalance capability can be evaluated by

$$\varepsilon_{max} = \frac{P_{j,max}}{\frac{1}{n}P} = \frac{M_{j,max}}{M_n}. \tag{7}$$

From the above (7), the maximum power imbalance is determined by a ratio between the nominal modulation index and the maximum modulation index. As one possibility to extend the capability, the nominal modulation index can be reduced. This is achieved by increasing the DC-link voltage. However, the increased voltage would lead to not only over-designed system such as over-rated devices but also decreased power quality or strict filter requirement. Another possibility is to extend the maximum modulation index. This motivates to explore a modulation strategy.

III. Proposed Modulation

By the conventional modulation method [12], [26], the maximum modulation index is limited to 1 (i.e. $M \in [0,1]$). In this section, a novel modulation strategy to extend the power imbalance capability is proposed, which is based on discontinuous modulation. The proposed method is applied to single-phase CHB inverters with the phase-shifted carriers.

A. Principle

The conventional discontinuous modulation methods have been typically studied to improve power conversion efficiency in three-phase systems [27]. However, in this work, a new discontinuous modulation is proposed, which is applied to single-phase CHB inverter and aims at extending the power imbalance capability among cells in a phase.

The proposed method is shown in Fig. 3, which has two variants of signal: Fig. 3 (a) clamped signal m_c for additional power (ε>1) and Fig. 3 (b) non-clamped signal m_{nc} for reduced power (ε<1). The basic concept is that each modulation signal is applied to a respective cell according to power imbalance requirements. Namely, an additional loading cell is modulated by the clamped signal, whereas an unloading cell is operated with the non-clamped signal.

This article has been accepted for publication in a future issue of this journal, but has not been fully edited. Content may change prior to final publication. Citation information: DOI 10.1109/TPEL.2021.3065028, IEEE Transactions on Power Electronics

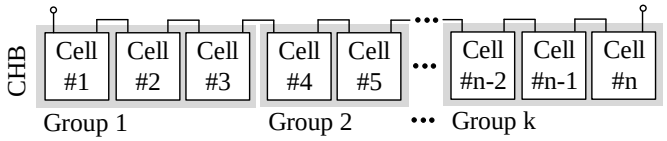

Fig. 4: Generalization by grouping n cells with either two cells or three cells.

The proposed signals can be obtained by utilizing a same fundamental offset component m_o as expressed as

$$\begin{cases} m_c(\varphi,\alpha) = m_n + m_o(\varphi,\alpha) \\ m_{nc}(\varphi,\alpha) = m_n - m_o(\varphi,\alpha). \end{cases} \tag{8}$$

where m_n is a sinusoidal signal with modulation index of M_n, i.e. $m_n = M_n sin(\theta)$, where θ is the angle. Here, m_o is symmetric with respect to α, i.e. it has non-zero value in the phase internal $[0.5\pi+\alpha-0.5\varphi,\ 0.5\pi+\alpha+0.5\varphi]$ and $[1.5\pi+\alpha-0.5\varphi,\ 1.5\pi+\alpha+0.5\varphi]$.

From (8) and considering a system with two cells, it should be noted that the offset components are completely compensated. Hence, a summation of two modulation signals has only the fundamental component m_n, which implies that the total inverter voltage V_{inv} does not feature the offset voltage.

On the other hand, as shown in Fig. 3, there are two control variables: the clamping angle φ and the shifting angle α. The clamping angle mainly affects the degree of power imbalance, while the shifting angle is determined in accordance with the power factor. The influence of these two variables will be analyzed in detail in section IV.

B. Generalization

The principle of the proposed method was previously presented, considering a system with two cells. However, considering various power imbalance scenarios in a system with a higher number of cells, the proposed method needs to be generalized for a practical implementation of the algorithm.

First, the system with higher number of cells can be regarded as a system with cell groups, in which the cell group consists of either two cells or three cells. Namely, there are two basic groups, one is with two cells and another is with three cells. For a better understanding, an example is shown in Fig. 4, where a system with n cells are considered and all of cells is regarded as k groups. Here, the only requirement for composing the groups is that every cell must be involved in one of the groups. By this grouping means, any systems can be addressed with combination of the basic groups. Once a system under consideration is restructured by multiple groups, the proposed method can be *individually* implemented to each group. This means that the application of the proposed method to a respective group does not interfere other groups. Therefore, the proposed method can be simply implemented without any restriction of the number of cells. For a better understanding, an example system is considered, which consists of five cells and their loading powers are unbalanced as shown in Fig. 5 (a). First, in order to satisfy the requirement, two groups should be comprised: one group

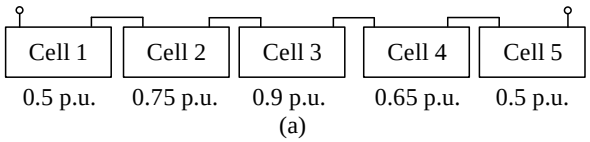

(a)

* Abbreviation of Strategy: Str

1	Cell 1 & 2	Str 1	6	Cell 2 & 4	Str 1
	Cell 3, 4, & 5	Str 2		Cell 1, 3, & 5	Str 2
2	Cell 1 & 3	Str 1	7	Cell 2 & 5	Str 1
	Cell 2, 4, & 5	Str 3		Cell 1, 3, & 4	Str 2
3	Cell 1 & 4	Str 1	8	Cell 3 & 4	Str 1
	Cell 2, 3, & 5	Str 2		Cell 1, 2, & 5	Str 2
4	Cell 1 & 5	Str 1	9	Cell 3 & 5	Str 1
	Cell 2, 3, & 4	Str 2		Cell 1, 2, & 4	Str 3
5	Cell 2 & 3	Str 1	10	Cell 4 & 5	Str 1
	Cell 1, 4, & 5	Str 2		Cell 1, 2, & 3	Str 3

(b)

Fig. 5: An example of grouping method of a system with five cells: (a) loading power of each cell and (b) ten possible grouping candidates and respective strategy shown in Fig. 6.

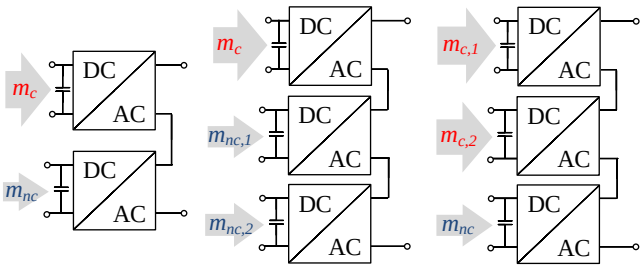

(a) (b) (c)

Fig. 6: Possible power imbalance strategies, considering the basic groups: (a) two cells (strategy 1) and three cells of (b) one additional loading cell and two unloading cells (strategy 2) or (c) two additional loading cells and one unloading cell (strategy 3).

is with two cells and another group should involve remaining three cells. Hence, ten possible combinations exist in total as listed in Fig. 5 (b) and one candidate can be randomly chosen. Finally, once the grouping is performed, the power imbalance strategy is applied to each group. In the following, the three strategies are addressed.

As the simplest case, the two cell is considered, which is shown in Fig. 6 (a). Here, one of both has additional power loading, whereas another one processes a reduced power. To accomplish this power imbalance, the modulation presented in (8) can be directly employed.

The possible power imbalance cases with three cells are shown in Fig. 6 (b) and (c). In case of Fig. 6 (b), one cell is additionally loaded and the others are unloaded. Further, the two cells could be differently unloaded. This power imbalance scenario is handled with three modulation signals, which are

expressed in

$$\begin{cases} m_c(\varphi,\alpha) = m_n + m_o(\varphi,\alpha) \\ m_{nc,1}(\varphi,\alpha) = m_n - \left(\frac{1}{\gamma}\right) m_o(\varphi,\alpha) \\ m_{nc,2}(\varphi,\alpha) = m_n - \left(1-\frac{1}{\gamma}\right) m_o(\varphi,\alpha). \end{cases} \tag{9}$$

Here, the identical clamping angle φ and the shifting angle α are employed for all modulation signals. However, the different coefficients are used for each unloaded cell in order to ensure the individual power loading control of the cells, where the coefficients are determined by the factor γ ($\gamma \geq 1$). Namely, the total unloading power is distributed between two unloading cells, $m_{nc,1}$ and $m_{nc,2}$, by means of determining γ. For example, when γ is 3, the power of $m_{nc,1}$ is 1/3 of the total power, while that of $m_{nc,2}$ is 2/3. Like in the case for two cells, the offset components are completely compensated to ensure only the fundamental component in the total voltage.

The principle to choose numerical value of γ is explained in the following. First of all, it is assumed that the mean power of the group P_{mean} is 1 [p.u.] for simplicity. Hence, the total power of the group P is 3 [p.u.]. Second, the total additional loading power by one cell ΔP and the total unloading by two cells $-\Delta P$ must be identical. Therefore, the power of the additional loading cell is $1+\Delta P$ [p.u.] and the power of two unloading cells is $2-\Delta P$ [p.u.]. Finally, the unloading power $-\Delta P$ needs to be distributed to two unloading cells, $-\Delta P = -(\Delta P_1 + \Delta P_2)$. Hence, the loading power of two cells can be expressed as $1-\Delta P_1$ [p.u.] and $1-\Delta P_2$ [p.u.]. From this, the numerical value of γ can be determined by applying $(\Delta P_1 + \Delta P_2)/\Delta P_1$.

The final case is shown in Fig. 6 (c), in which two cells are additionally loaded and one cell is unloaded. Therefore, three modulation signals need to be employed: two are clamped signals and one is non-clamped signal. These are shown in (10).

$$\begin{cases} m_{c,1}(\varphi_1,\alpha_1) = m_n + m_o(\varphi_1,\alpha_1) \\ m_{c,2}(\varphi_2,\alpha_2) = m_n + m_o(\varphi_2,\alpha_2) \\ m_{nc}(\varphi,\alpha) = m_n - [(m_o(\varphi_1,\alpha_1) + m_o(\varphi_2,\alpha_2)] \end{cases} \tag{10}$$

The clamping angle for each clamped signal is different and this is determined by the power imbalance ε for each cell. Then, the non-clamped signal is generated with the relation to the clamped signals. Of course, the offset components are completely compensated.

IV. Analysis of the Proposed Method

By increasing the amount of injected active power into the grid, the amplitude of the grid voltage possibly violates the limitation defined in the grid code [28], [29]. In this regard, the CHB inverter is supposed to support the grid voltage by means of reactive power compensation. Therefore, in this section, the capability of the proposed method is analyzed, considering operation with the unity power factor and operation with non-unity power factor.

A. Power Imbalance

As mentioned before, the proposed method has two control parameters, the clamping angle φ and the shifting angle α. The influence of these two parameters on the power imbalance is analyzed. To do so, the fundamental component of the proposed signals in Fig. 3 needs to be derived, because only the fundamental component (e.g. 50/60 Hz in grid connected inverters) contribute to a power transfer between AC and DC ports.

Since the proposed signals are periodic, the fundamental component of the modulation signals can be derived with the first-order coefficients of Fourier series. The first-order coefficients are expressed in (11).

$$\begin{cases} a_1 = \frac{1}{\pi}\int_{\theta_1}^{\theta_2} f(\theta)cos(\theta)d\theta \\ b_1 = \frac{1}{\pi}\int_{\theta_1}^{\theta_2} f(\theta)sin(\theta)d\theta \end{cases} \tag{11}$$

where a_1 and b_1 are the Fourier coefficients for the fundamental component, θ is the angular frequency of the fundamental component and $f(\theta)$ is the target signal function. Here, the target signal is the clamped signal m_c shown in Fig. 3 (a) and this is described in (12).

$$f(\theta) = \begin{cases} 1, \quad \text{when } [0.5\pi+\alpha-0.5\varphi,\ 0.5\pi+\alpha+0.5\varphi] \\ M_n \cdot sin(\theta), \\ \qquad\qquad \text{when } [0,\ 0.5\pi+\alpha-0.5\varphi], \\ \qquad [0.5\pi+\alpha+0.5\varphi,\ 1.5\pi+\alpha-0.5\varphi], \\ \qquad [1.5\pi+\alpha+0.5\varphi,\ 2\pi] \\ -1, \\ \quad \text{when } [1.5\pi+\alpha-0.5\varphi,\ 1.5\pi+\alpha+0.5\varphi] \end{cases} \tag{12}$$

Consequently, the fundamental component F_c can be obtained as shown in (13) [30].

$$F_c(\varphi,\alpha) = \sqrt{a_1^2(\varphi,\alpha) + b_1^2(\varphi,\alpha)} \tag{13}$$

where

$$\begin{cases} a_1 = 4sin\left(\frac{\varphi}{2}\right) sin(\alpha) - M_n\varphi + M_n\pi \\ \qquad + 4M_n cos\left(\frac{\varphi}{2}\right) sin\left(\frac{\varphi}{2}\right) cos(\alpha)^2 \\ b_1 = 4sin\left(\frac{\varphi}{2}\right) cos(\alpha)\left(M_n cos\left(\frac{\varphi}{2}\right) sin(\alpha) - 1\right). \end{cases} \tag{14}$$

Here, a_1 and b_1 are the coefficient of cosine and sine term, respectively. As it can be seen, the fundamental component is a function of the clamping angle and the shifting angle.

On the other hand, the fundamental component of non-clamped signal is dependent on the three power imbalance control strategies presented in III-B. The fundamental component under different strategies are found as below equations, where (15) is for the strategy 1, (16) is for the strategy 2 and (17) presents the strategy 3. For better understanding, the fundamental component of non-clamped signal for the strategy 1 is obtained by subtracting F_c from the total nominal modulation index of two cells $2M_n$. In the same way, the

This article has been accepted for publication in a future issue of this journal, but has not been fully edited. Content may change prior to final publication. Citation information: DOI 10.1109/TPEL.2021.3065028, IEEE Transactions on Power Electronics

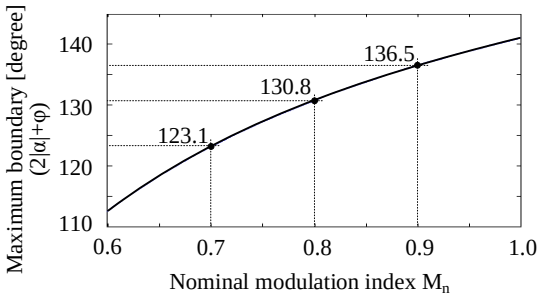

Fig. 7: Maximum limitation of strategy 3 depending on the nominal modulation index as expressed in (A-5).

fundamental component of non-clamped signal for the strategy 2 and 3 can be obtained, considering three cells.

$$F_{nc}(\varphi,\alpha) = 2M_n - F_c(\varphi,\alpha) \tag{15}$$

$$\begin{cases} F_{nc,1}(\varphi,\alpha) = M_n - \dfrac{1}{\gamma}\left(F_c(\varphi,\alpha) - M_n\right) \\ F_{nc,2}(\varphi,\alpha) = M_n - \left(1 - \dfrac{1}{\gamma}\right)\left(F_c(\varphi,\alpha) - M_n\right) \end{cases} \tag{16}$$

$$F_{nc}(\varphi,\alpha) = 3M_n - \left(F_{c,1}(\varphi_1,\alpha) + F_{c,2}(\varphi_2,\alpha)\right) \tag{17}$$

The clamping angle can be varied between [0, π], however, referring to [31] the constraint on the maximum clamping angle must be considered for the analysis. For the strategy 1 and 2, there is no constraint, i.e. the clamping angle can be controlled in the full range. The constraint is occurred for the strategy 3 due to over-modulation of the non-clamped signal. Showing (10), there are two clamped signals, which have a respective clamping angle φ_1 and φ_2. One of the clamping angles can be controlled in the interval [0, π], while another one can be varied in [0, $2arccos(1/(3M_n)) - \alpha$]. For example, when M_n is 0.8 and α is 0, it is $2.28\,rad$ ($\approx 130.8°$). This constraint is derived in detail in the appendix I. The maximum boundary value as a function of the nominal modulation index is analyzed in Fig. 7, which is $2|\alpha|+\varphi$. The higher nominal modulation index allows the higher maximum boundary value. However, it does not imply the higher power imbalance capability, since the capability is determined by the relation in (7).

Based on (13) and (15), the power imbalance capability for the strategy 1 is shown in Fig. 8 as a function of the clamping angle and shifting angle, where Fig. 8 (a) is for additional loading and Fig. 8 (b) is for reduced loading. Here, a nominal modulation index of 0.8 is considered. By increasing the clamping angle up to 180°, the fundamental component $m_{j,max}$ is increased up to $4/\pi$ ($\approx$1.273). Therefore, the maximum power ε_{max} in (7) is 1.59 [p.u.] as shown in Fig. 8 (a). The minimum power of 0.41 [p.u.] is achieved as shown in Fig. 8 (b). Further, it is noting that the conventional method can achieve ε_{max} of 1.25 by (7). This is displayed by white-dot line in Fig. 8 (a), clearly demonstrating the extended power imbalance capability by the proposed method.

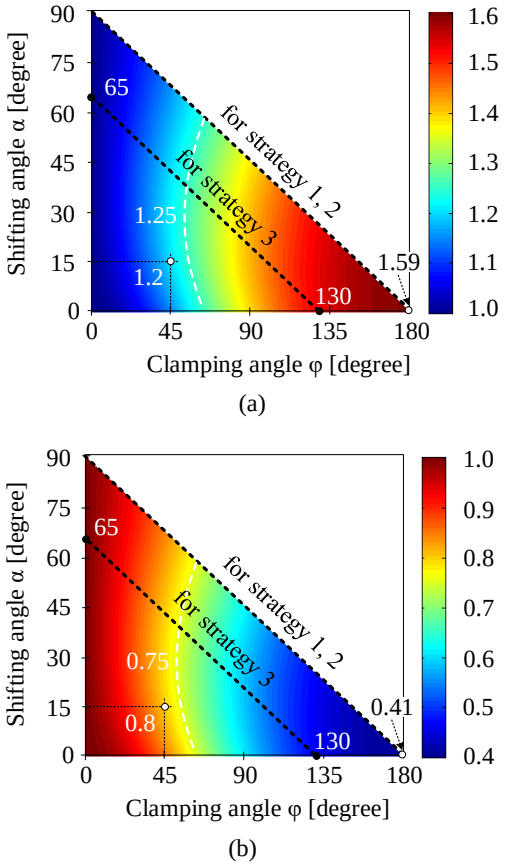

Fig. 8: Power imbalance capability ε: (a) additional loading and (b) unloading ($M_n = 0.8$).

As shown in Fig. 8, the loading power is determined by the clamping and shifting angles. However, it can be noticed that the clamping angle mainly affects the loading power with respect to the shifting angle in case the range of shifting angle is between $30-70\%$ of the maximum available shifting angle. For example, the operating condition is ($\varphi = 45°$, $\alpha = 30°$) with assumption of there variation is $\pm 5°$ (i.e. $\Delta\varphi = \Delta\alpha = \pm 5°$). In this case, the additional loading power obtained with Fig. 8 (a) is summarized in the below:

- $\varphi = 45°$ and $\alpha = 30°$ $\Rightarrow$ 1.214 [p.u.] (-)
- $\varphi = 50°$ and $\alpha = 30°$ $\Rightarrow$ 1.237 [p.u.] ($\uparrow$ 1.89 %)
- $\varphi = 40°$ and $\alpha = 30°$ $\Rightarrow$ 1.189 [p.u.] ($\downarrow$ 2.06 %)
- $\varphi = 45°$ and $\alpha = 35°$ $\Rightarrow$ 1.211 [p.u.] ($\downarrow$ 0.25 %)
- $\varphi = 45°$ and $\alpha = 25°$ $\Rightarrow$ 1.213 [p.u.] ($\downarrow$ 0.08 %)

On the other hand, when the shifting angle is out of the range, the impact of the shifting angle is increased. For example in case the operating condition is ($\varphi = 45°$, $\alpha = 15°$), the additional loading is as below:

- $\varphi = 45°$ and $\alpha = 15°$ $\Rightarrow$ 1.2 [p.u.] (-)
- $\varphi = 50°$ and $\alpha = 15°$ $\Rightarrow$ 1.227 [p.u.] ($\uparrow$ 2.25 %)
- $\varphi = 40°$ and $\alpha = 15°$ $\Rightarrow$ 1.175 [p.u.] ($\downarrow$ 2.08 %)
- $\varphi = 45°$ and $\alpha = 20°$ $\Rightarrow$ 1.209 [p.u.] ($\downarrow$ 0.75 %)
- $\varphi = 45°$ and $\alpha = 10°$ $\Rightarrow$ 1.188 [p.u.] ($\downarrow$ 1.0 %)

Consequently, the loading power is dependent on both

angles, but it is further influenced by the clamping angle. Moreover, the shifting angle is determined by power factor in order to achieve the optimized efficiency (this will be discussed in the next section *CHB Inverter Efficiency*).

The capability for the strategies 2 and 3 can be simply derived based on Fig. 8. For the strategy 2, the capability of unloading cells is obtained with the factor γ, while that of additional loading is identical with the strategy 1. For the strategy 3, Fig. 8 (a) is applied to each additional loading cell, then, unloading is calculated by a summation of both additional loading cases. Here, the maximum modulation index for strategy 3 in Fig. 8 is derived for $M_n = 0.8$. Therefore, the available maximum clamping angle of one additional loading cell is limited by 130.8° as shown in Fig. 7. It should be noted that even though three cells are considered for the strategies 2 and 3, Fig. 8 can be applied to analyze the loading power. This is because the impact of cells on the loading power is independent of each other. Namely, the loading power of each cell is solely determined by its clamping and shifting angles.

For a better understanding, an example case is described: For the strategy 1, the operating condition of ($\varphi = 45°$, $\alpha = 15°$) is considered as shown in Fig. 8. Hence, the power imbalance of $\varepsilon = (1.2, 0.8)$ is realized. Considering the identical condition with $\gamma = 4$ for the strategy 2, $\varepsilon = (1.2, 0.95, 0.85)$ is obtained. Finally, for the strategy 3, under the operating condition ($\varphi = 45°$, $\alpha = 15°$), ($\varphi = 180°$, $\alpha = 0°$), the obtained power imbalance is $\varepsilon = (1.2, 1.59, 0.21)$.

B. CHB Inverter Efficiency

The efficiency of CHB inverters is highly influenced by the modulation strategy. Especially, the discontinuous modulation schemes inherently obtain lower switching losses with the clamped behavior. In order to analyze the influence of the proposed method on loss distribution, the average loss model is employed [32].

$$\begin{cases} P_{sw} = \left[\dfrac{1}{2\pi} \dfrac{V_{dc}}{V_{base}} \displaystyle\int_{\theta_1}^{\theta_2} \left(a i_c^2 + b i_c + c \right) d\theta \right] f_{sw} \\ P_{cd} = \dfrac{1}{2\pi} \displaystyle\int_{\theta_1}^{\theta_2} \delta i_c V_{ce} d\theta \end{cases} \tag{18}$$

Thereby P_{sw} and P_{cd} are the switching and conduction losses, respectively, f_{sw} is the switching frequency, V_{dc} is the DC-link voltage, V_{base} is the reference DC-link voltage used to obtain the $E_{sw} - I_c$ curve in the data-sheet and a, b and c are curve fitting constants. δ is the modulation function and V_{ce} is the on-state voltage.

In the following, the loss distribution is analyzed with the above loss model, considering only the clamped signal. This is because the non-clamped signal hardly influences the loss distribution, whereas the influence of the clamped signal is significant as presented in [31].

The loss distribution with the clamped signal is analyzed in Fig. 9 under different power factors, in which Fig. 9 (a) is with the unity power factor $cos(\varphi) = 1$, Fig. 9 (b) is with $cos(\varphi) = 0.66$ and Fig. 9 (c) presents with $cos(\varphi) = 0.33$. Of course, system operation with such low power factor could be restricted by grid operator, however, in order to clearly show impact of the proposed method, extreme cases are considered. For each case, the influence of clamping angle and shifting angle can be identified. As it can be seen, the clamping angle affects the loss distribution, since it highly contributes for power loading as analyzed in previous section. It is reasonable to conclude that different power affects the loss distribution for all cases. On the other hand, the contribution of shifting angle is non-negligible as well. Furthermore, its influence is dependent on the power factor, i.e. reactive power compensation strategy.

For the unity power factor shown in Fig. 9 (a), as increasing the shifting angle with a fixed specific clamping angle, the losses are becoming higher. This means that the minimum losses can be achieved with 0° shifting angle for all clamping angles. On the other hand, for the second (in Fig. 9 (b)) and third (in Fig. 9 (c)) case, the losses are decreasing for higher shifting angles. At a certain point, they increase again. Therefore, it can be noticed that the shifting angle for the minimum losses is moved from 0° to the certain point. For the case with $cos(\varphi) = 0.66$ power factor, the current is delayed by 30° in respect to the voltage, the minimum losses are shown with shifting angle between [25°, 30°]. In case of $cos(\varphi) = 0.33$, the shifting angle between [55°, 60°] enables the minimum losses. From this analysis, it can be noticed that the losses are dependent on the shifting angle. Remarkably, the minimum losses are achieved when the clamped angle is centered at the peak current. In other words, when the shifting angle is identical with a power factor angle, because the switching losses are proportional to the peak current.

To sum up the analysis of both power imbalance capability and loss distribution, the clamping and shifting angles need to be properly chosen, considering a requirement of power imbalance together with achieving a higher efficiency. For the higher efficiency, the shifting angle is first determined by power factor that is determined with reactive power compensation strategy, then, the clamping angle is chosen to perform a required power imbalance with the designated shifting angle.

C. Power Quality

The power quality is one of the most important criteria to evaluate power converter's performance. The CHB inverters are typically advantageous to achieving high power quality with higher equivalent switching frequency. However, this advantage is taken only when the system operating condition is identical, i.e. balanced DC-link voltage and modulation signal for each cell [33], [34]. The proposed method technically exploits unequal modulation signal to perform the power imbalance, which would lead to an inferior power quality. Hence, the influence of the proposed method on the power quality needs to be investigated.

Referring [35], the inverter output voltage v_{inv} is regenerated through the Fourier series as shown in (19) and (20).

$$v_{inv}(t) = \sum_{j=1}^{n} v_j(t) \tag{19}$$

This article has been accepted for publication in a future issue of this journal, but has not been fully edited. Content may change prior to final publication. Citation information: DOI 10.1109/TPEL.2021.3065028, IEEE Transactions on Power Electronics

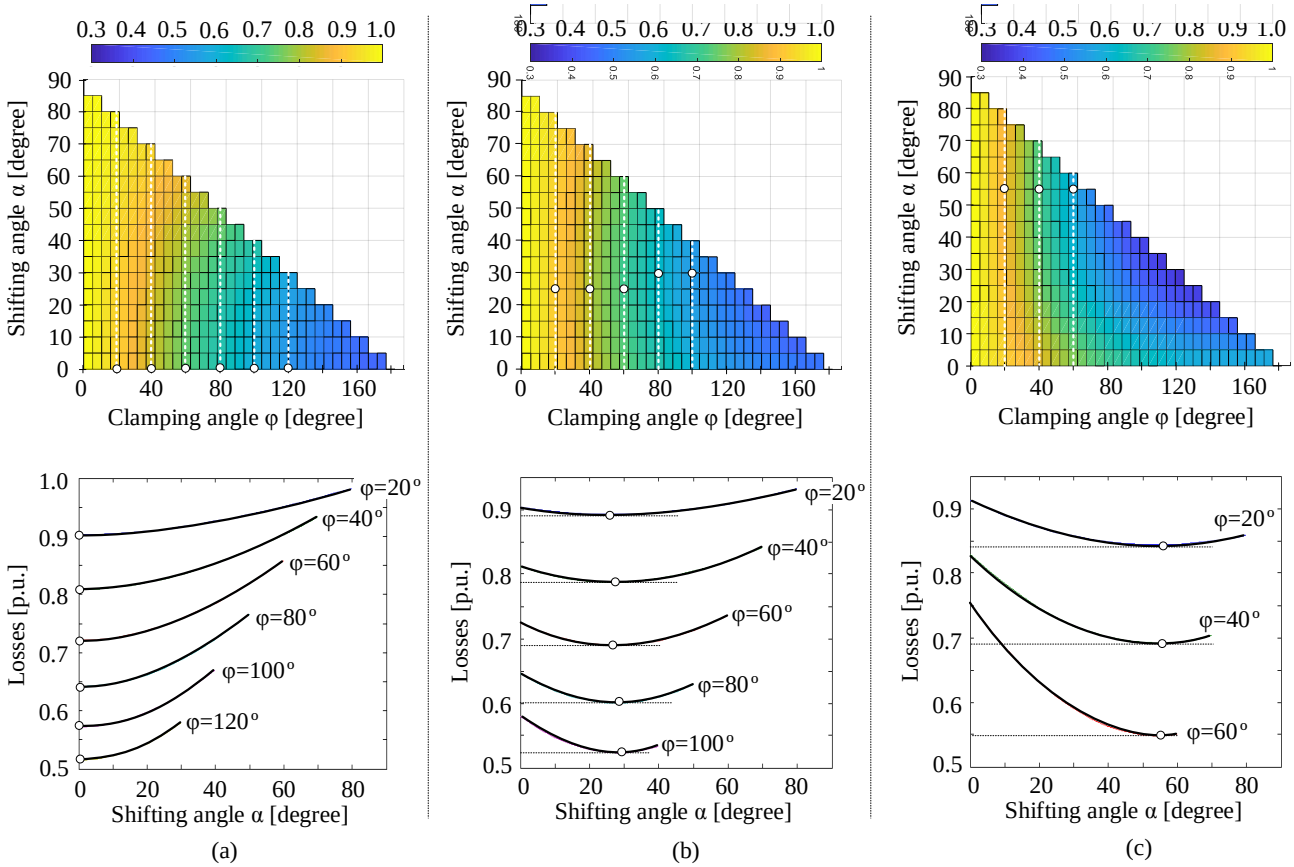

Fig. 9: Loss distribution with clamped signal for different power factors: (a) $cos(\varphi) = 1$ (0°), (b) $cos(\varphi) = 0.66$ (30°) and (c) $cos(\varphi) = 0.33$ (60°) (the losses are represented in per unit of the value when $\varphi = 0°$ and $\alpha = 0°$, circle: minimum losses with a specific clamping angle).

where

$$v_j(t) = V_{dc} m_j + \frac{2V_{dc}}{\pi} \sum_{k=1}^{\infty} \frac{sin(k\pi m_j) cos(k\omega_c t + \theta_j)}{k}. \quad (20)$$

Here, v_j is the cell voltage, ω_c is the carrier frequency and θ_j is the carrier phase angle. Then, the Total Harmonic Distortion (THD) is calculated from the regenerated signal. In the following, a system with eight cells, e.g. $n = 8$, is considered and each strategy is applied for a basic group for the sake of simplicity. Namely, a group having two cells is operated for the strategy 1, while the others are operated with sinusoidal modulation. In the same way, the other strategies are applied. In addition, γ=2 for the strategy 2 and φ_1=φ_2 for the strategy 3 are considered. Hence, for the strategy 3, the maximum available clamping angle is limited to 130°. With such assumption, this analysis does not represent the overall performance with the proposed method. However, it would be valuable to show the trend of power quality as increasing the degree of the power imbalance.

Fig. 10 shows the normalized performance in dependence of the clamping angle and the shifting angle, where Fig. 10 (a) is with strategy 1, Fig. 10 (b) is with strategy 2 and Fig. 10 (c) is with strategy 3. For all cases, the performance becomes worse with a wider angles. The strategies 1 and 2 show similar performance (maximum THD is 1.68 and 1.64 p.u.), while the strategy 3 further negatively affects the performance, showing 1.91 p.u. of the maximum THD. The line for 1.2 p.u. THD is indicated, which shows the trend of performance with different angles.

The performance is compared with the conventional sinusoidal method as a function of power imbalance ε, considering the identical system with Fig. 10, where the conventional method modifies only the amplitude of sinusoidal modulation signal in dependence of the power. The result is shown in Fig. 11, where x-axis represents the degree of power imbalance and y-axis is the relative THD. Here, it is noted that $\varepsilon = 0$ represents the balanced power and the higher ε means the heavier power imbalance. As increasing the power imbalance, the performance is decreased by both methods. Showing Fig. 11 (a), the power imbalance of 1.25 p.u. is the maximum value with the conventional method at the expense of 30% decreased power quality. Here, the maximum power imbalance capability of the conventional method is obtained by (7). The proposed method instead extends the power imbalance upto 1.59 p.u. with 68% decreased THD performance. Further, it is remarkable that in the range of $1.0 < \varepsilon < 1.25$, the THD with the proposed method shows the similar or even better performance. At $\varepsilon = 1.25$, THD is 1.3 with the conventional method, while it is 1.17 with the proposed method (around 10 % improved). The THD with the strategies 2 and 3 exhibits

This article has been accepted for publication in a future issue of this journal, but has not been fully edited. Content may change prior to final publication. Citation information: DOI 10.1109/TPEL.2021.3065028, IEEE Transactions on Power Electronics

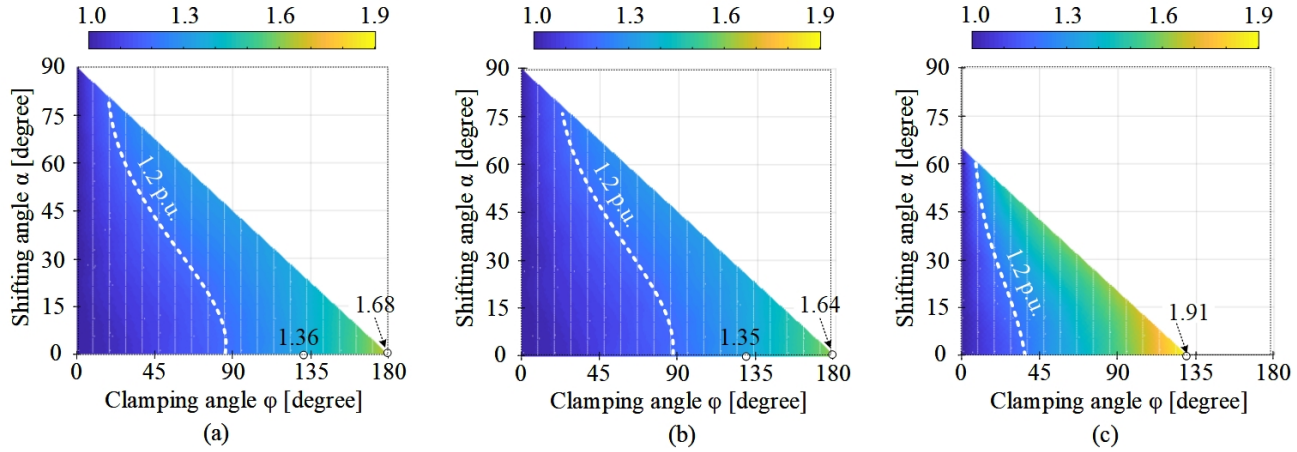

Fig. 10: THD performance with the proposed method, considering a system of $n = 8$: (a) strategy 1, (b) strategy 2 and (c) strategy 3 (the THD is represented in per unit of the value when $\varphi = 0°$ and $\alpha = 0°$, $M_n = 0.8$).

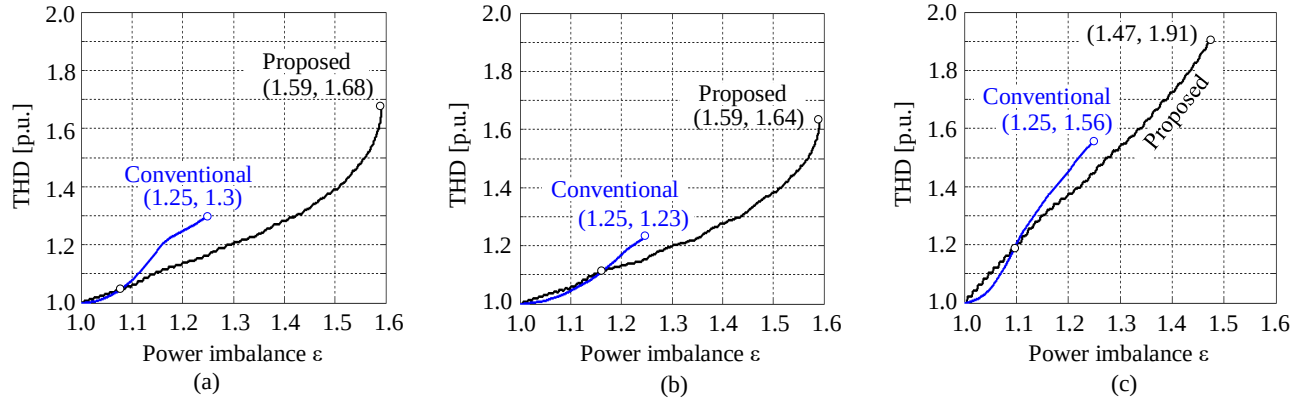

Fig. 11: Comparison of THD performance between conventional and proposed method (α=0°): (a) strategy 1, (b) strategy 2 and (c) strategy 3 (the THD is represented in per unit of the value when $\varphi = 0°$ and $\alpha = 0°$, $M_n = 0.8$).

the similar trend as shown in Fig. 11 (b) and (c), respectively.

To sum up, the proposed method can significantly extend the power imbalance capability compared with the conventional method, while showing the similar (slightly lower or higher) or better THD depending on the power imbalance.

V. Implementation

In order to validate the feasibility of the proposed method, it is implemented to feedback controller of the whole system consisting PV model, DC-DC converters and CHB converter.

Fig. 12 shows the control scheme for the DC-DC converters and for the CHB converter, where the system consists n cells. The DC-DC converters are responsible for the DC-link voltage control as shown in Fig. 12 (a), where V^*_{dc} is the reference voltage, $v_{dc,x}$ is the measured voltage and φ_x represents the phase shift angle ($x = 1, 2, ..., n$). Here, the dual active bridge converters operated with the phase shift control [36], are employed as the DC-DC converters. On the other hand, the CHB converter performs the Maximum Power Point Tracking (MPPT) algorithm, leading to the grid current reference I^*_g. Here, $v_{pv,x}$, $i_{pv,x}$ and $p_{pv,x}$ are the voltage, current, power of x^{th} PV string and p_{pv} is the total generated power. By employing the analysis in Figs. 4 and 8, the clamping and shifting angles are calculated, depending on the power imbalance requirements ε_x. Finally, the final modulation signals m_x are obtained with the output of the current controller m_{avg}, φ_x and α_x. The entire control scheme for the CHB is shown in Fig. 12 (b).

The control scheme is implemented in the system with 3 cells and the result waveforms are shown in Fig. 13, where Fig. 13 (a) is voltage of PV strings, Fig. 13 (b) is the grid voltage and current, Fig. 13 (c) is the DC-link voltage of CHB and Fig. 13 (d) represents the modulating signals. In case the generated power is balanced (before 0.1sec), PV voltages and the modulating signals for all cells are identical. At the 0.1sec, the generated power from the PV strings becomes uneven and $\varepsilon_{1,2,3} = [1.2, 0.95, 0.85]$. The PV voltages become 1 [p.u.], 0.94 [p.u.] and 0.8 [p.u.] due to different MPPs, while the DC-link voltages are kept equally. Remarkably, in order to handle the power imbalance, the modulating signals are modified with the clamping and shifting angles, employing the strategy 2. Hence, one cell is clamped and the others are modulated with the non-clamped signal. Finally, as it is seen, the operating point from the sinusoidal method to the proposed method is

This article has been accepted for publication in a future issue of this journal, but has not been fully edited. Content may change prior to final publication. Citation information: DOI 10.1109/TPEL.2021.3065028, IEEE Transactions on Power Electronics

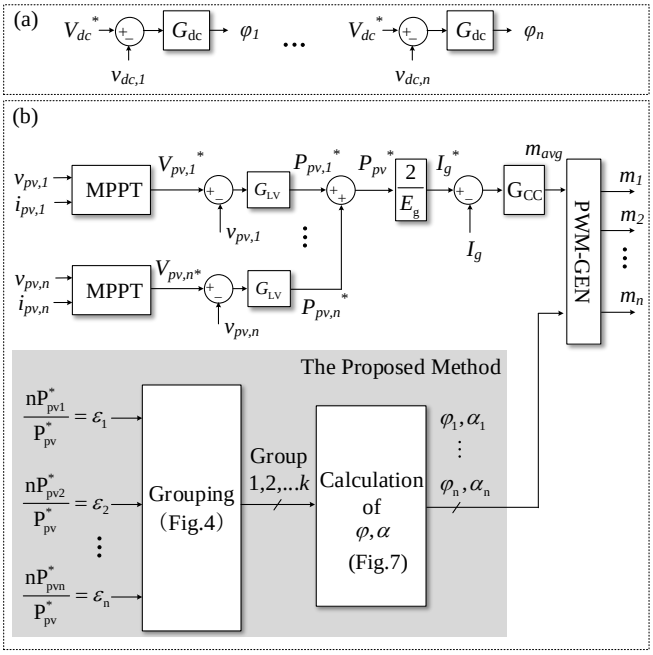

Fig. 12: Control scheme: (a) DC-DC converters and (b) CHB converter.

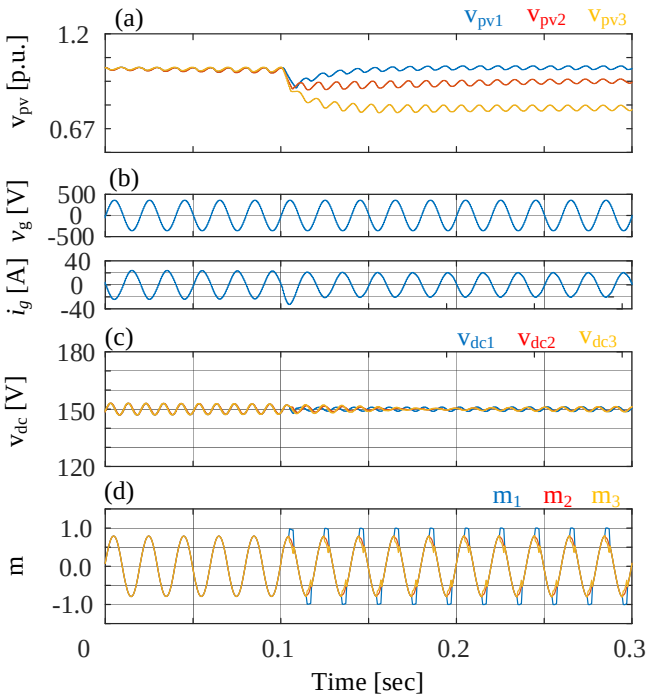

Fig. 13: Simulation waveforms: (a) voltage of PV strings, (b) grid voltage and current, (c) DC-link voltage of cells and (d) modulating signals of cells.

seamlessly transferred, without affecting control performance.

VI. Experimental Validation

The proposed method is validated in terms of its power imbalance capability, efficiency and power quality. The developed setup consists of 3 cells, where the cells are individually

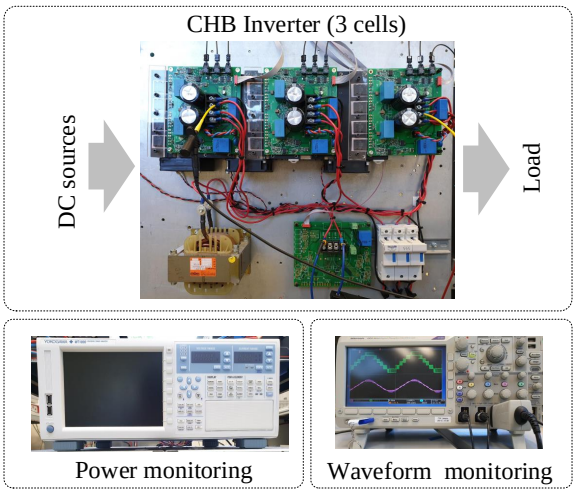

Fig. 14: Developed experimental setup consisting of 3 cells.

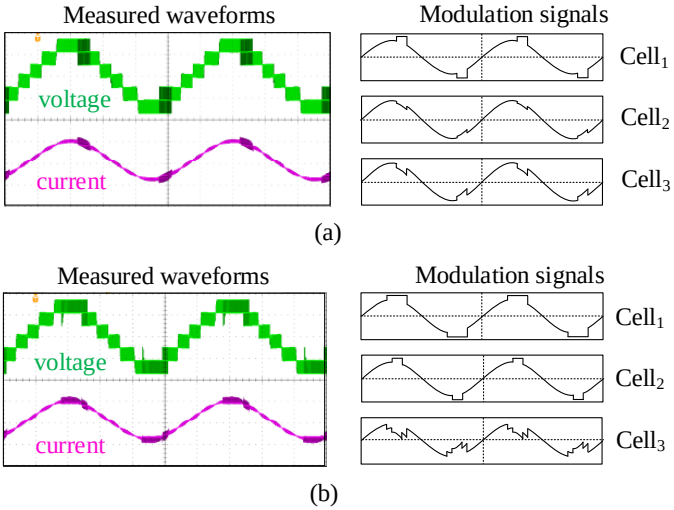

Fig. 15: Experiment inverter voltage and current waveforms with (a) strategy 2 (φ=30°, α=30°, γ=3) and (b) strategy 3 (φ_1=30°, φ_2=60°, α=15°).

supplied by its respective DC source and the nominal modulation index of 0.8 is applied. The input power (DC power of each cell) and the output power (AC power) are monitored with a power analyzer 'Yokogawa WT3000E', and the AC voltage and AC current are measured with an oscilloscope 'Tektronix DPO3014' as shown in Fig. 14.

First of all, the feasibility is confirmed in Fig. 15, where the inverter voltage and current are shown together with corresponding modulation signals. The voltage and current are always sinusoidal when the strategy 2 and 3 are applied as shown in Figs. 15 (a) and (b), respectively. Here, the power factor is $cos(\varphi) = 0.98$.

The power imbalance capability is validated in Fig. 16, by comparing the transferred power of each cell. Fig. 16 (a) shows the power imbalance when the strategy 2 with γ=4 is applied, where the left figure is for an additional loading cell and the middle and right figures are for unloading cells.

Here, the operating points are described as below.

- OP_1 : α=0° and φ=[0, 30, 60, 90, 120, 150, 180]°
- OP_2 : α=15° and φ=[0, 30, 60, 90, 120, 150]°
- OP_3 : α=30° and φ=[0, 30, 60, 90, 120]°
- OP_4 : α=45° and φ=[0, 30, 60, 90]°
- OP_5 : α=60° and φ=[0, 30, 60]°
- OP_6 : α=75° and φ=[0, 30]°

For all operating points, the degree of power imbalance ε is increasing with a wider clamping angle. Further, as setting the γ=4, the unloading cell #1 has the coefficient of 1/4 (1/γ in (16)) and the unloading cell #2 has 3/4 (1-1/γ). Hence, the loading power of the cell #2 is less than that of the cell #1. In addition, it is shown that the maximum power imbalance is performed between the additional loading cell and the unloading cell #2, when the clamping angle is 180° and the shifting angle is 0° in the OP1. In that case, the additional loading power is 234% higher the unloading power (=1.512/0.6455).

The power imbalance with the strategy 3 is shown in Fig. 16 (b), when the φ_1 is varied, whereas the φ_2 is fixed at 30°. The operating points for this case are as below.

- OP_1 : α=0°, φ_1=[0, 60, 90, 120, 150, 180]° and φ_2=30°
- OP_2 : α=15°, φ_1=[0, 60, 90, 120, 150]° and φ_2=30°
- OP_3 : α=30°, φ_1=[0, 60, 90, 120]° and φ_2=30°
- OP_4 : α=45°, φ_1=[0, 60, 90]° and φ_2=30°

Since the clamping angle for the second additional loading cell φ_2 is fixed at 30°, its loading power is constant unless the shifting is varied. On the other hand, the power for the additional loading of cell #1 and the unloaded cell is varied depending on the first clamping angle φ_1. As increasing φ_1, the degree of the power imbalance is increasing. The maximum power imbalance is 362% (=1.496/0.413) between the additionally loaded cell 1 and the unloaded cell, when the clamping angle is 180° as considered in OP1.

The impact of the proposed method is shown, when the strategy 2 with γ=2 is applied under the unity power factor. The x-axis is the shifting angle α and the y-axis is the normalized efficiency. The efficiency becomes higher with a wider clamping angle. Further, as shown in Fig. 9 (a), the higher efficiency is achieved when the shifting angle is zero unless the clamping is varied. This result is well matched with the theoretical analysis in Fig. 9 (a).

The THD of the inverter voltage is analyzed, when strategy 2 is applied with γ=2 and α=0°, as shown in Fig. 18. The experimental waveform is sampled trough the oscilloscope with 0.4 *usec* sampling time. The power quality is decreasing as the clamping angle is increased, as discussed in Fig. 10 and Fig. 11.

VII. Conclusion

The multi-string photovoltaic architecture is inevitably challenged by the mismatched operating conditions, leading to the unbalanced power among modules. For improving the power imbalance capability, and consequently the utilization of the PV modules, the discontinuous modulation based modulation has been introduced. The proposed grouping strategy enables the generalized implementation of the proposed modulation. The theoretical analysis demonstrates the capability of the power imbalance, the impact on the power efficiency and power quality. The maximum power imbalance capability is 59% of the full power with 56% reduced losses and 68% lower power quality, in respect of the sinusoidal modulation. The proposed method was validated in the experimental prototype in terms of potential power imbalance, its impact on the efficiency and power quality.

Appendix I: Constraint Derivation

Referring in [31], the constraint is occurred by non-clamped signal due to its over-modulation. The constraint of non-clamped signal for strategy 3 is addressed. The non-clamped signal is shown in Fig. A-1 to exemplify the constraint, assuming that $\varphi_1 \geq \varphi_2$.

In order to avoid over-modulation, the below conditions described in (A-1) must be satisfied.

$$\begin{cases} |\Delta m_1 - m_1| \leq 1 \\ |\Delta m_1 + \Delta m_2 - m_2| \leq 1 \end{cases} \tag{A-1}$$

where

$$\begin{cases} m_1 = M_n cos\left(\frac{\varphi_1}{2} + \alpha\right) \\ m_2 = M_n cos\left(\frac{\varphi_2}{2} + \alpha\right) \end{cases} \tag{A-2}$$

and

$$\begin{cases} \Delta m_1 = 1 - m_1 \\ \Delta m_2 = 1 - m_2. \end{cases} \tag{A-3}$$

By substituting (A-2) and (A-3) into (A-1), it can be re-written as

$$\begin{cases} \left|1 - 2M_n cos\left(\frac{\varphi_1}{2} + \alpha\right)\right| \leq 1 \\ \left|2 - 2M_n cos\left(\frac{\varphi_2}{2} - \alpha\right) + M_n cos\left(\frac{\varphi_1}{2} + \alpha\right)\right| \leq 1. \end{cases} \tag{A-4}$$

With the assumption of $\varphi_1 \geq \varphi_2$, φ_1 can be varied in the full range [0, π] *rad*, satisfying the first condition in (A-4). Therefore, only φ_2 is limited by the second condition in (A-4). By re-arranging the condition with assumption of $\varphi_1 = \varphi_2$, the constraint is consequently derived as

$$\varphi_2 \leq 2\left(cos^{-1}\left(\frac{1}{3M_n}\right) - \alpha\right). \tag{A-5}$$

References

[1] S. Rivera, S. Kouro, B. Wu, J. I. Leon, J. Rodriguez, and L. G. Franquelo, "Cascaded h-bridge multilevel converter multistring topology for large scale photovoltaic systems," in *2011 IEEE International Symposium on Industrial Electronics*, June 2011, pp. 1837–1844.

[2] A. I. Bratcu, I. Munteanu, S. Bacha, D. Picault, and B. Raison, "Cascaded dc-dc converter photovoltaic systems: Power optimization issues," *IEEE Transactions on Industrial Electronics*, vol. 58, no. 2, pp. 403–411, Feb 2011.

This article has been accepted for publication in a future issue of this journal, but has not been fully edited. Content may change prior to final publication. Citation information: DOI 10.1109/TPEL.2021.3065028, IEEE Transactions on Power Electronics

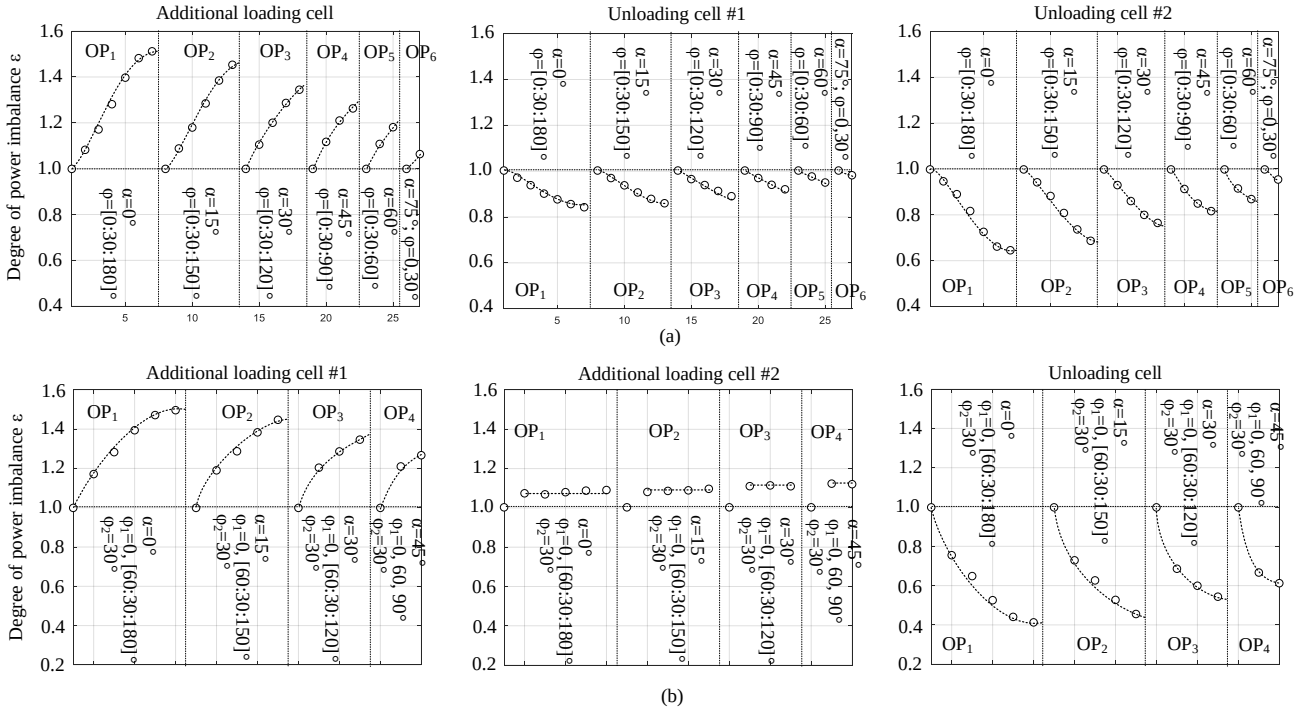

Fig. 16: Validation of power imbalance capability: (a) strategy 2 (φ=varied, α=varied, γ=4) and (b) strategy 3 (φ_1=varied, φ_2=30°, α=varied) (circle: measured, dot line: trend line).

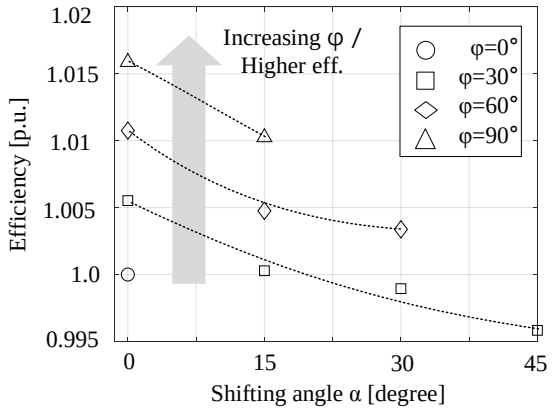

Fig. 17: Efficiency as a function of the shifting and clamping angles under the unity power factor (the efficiency is represented in per unit of the value when $\varphi = 0°$, markers: measured, dot line: trend line).

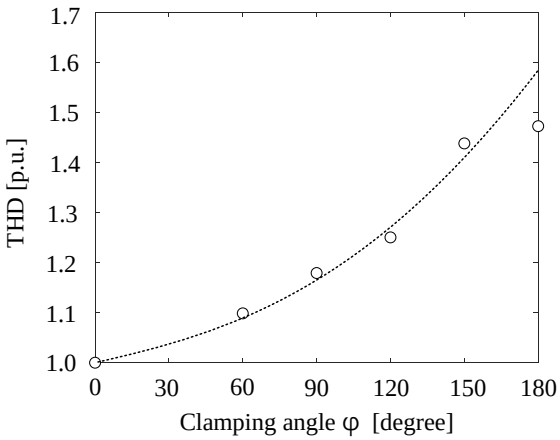

Fig. 18: THD performance with strategy 2 (γ=2 and α=0°) (the THD is represented in per unit of the value when $\varphi = 0°$, circle: measured, dot line: trend line).

[3] Y. Yu, G. Konstantinou, B. Hredzak, and V. G. Agelidis, "Power balance of cascaded h-bridge multilevel converters for large-scale photovoltaic integration," *IEEE Transactions on Power Electronics*, vol. 31, no. 1, pp. 292–303, Jan 2016.

[4] L. Maharjan, T. Yamagishi, and H. Akagi, "Active-power control of individual converter cells for a battery energy storage system based on a multilevel cascade pwm converter," *IEEE Transactions on Power Electronics*, vol. 27, no. 3, pp. 1099–1107, March 2012.

[5] P. Sochor and H. Akagi, "Theoretical comparison in energy-balancing capability between star- and delta-configured modular multilevel cascade inverters for utility-scale photovoltaic systems," *IEEE Transactions on Power Electronics*, vol. 31, no. 3, pp. 1980–1992, March 2016.

[6] K. Wang, R. Zhu, C. Wei, F. Liu, X. Wu, and M. Liserre, "Cascaded multilevel converter topology for large-scale photovoltaic system with balanced operation," *IEEE Transactions on Industrial Electronics*, vol. 66, no. 10, pp. 7694–7705, Oct 2019.

[7] B. Xiao, L. Hang, J. Mei, C. Riley, L. M. Tolbert, and B. Ozpineci, "Modular cascaded h-bridge multilevel pv inverter with distributed mppt for grid-connected applications," *IEEE Transactions on Industry Applications*, vol. 51, no. 2, pp. 1722–1731, March 2015.

[8] P. Sochor and H. Akagi, "Which is more suitable to a modular multilevel sdbc inverter for utility-scale pv applications, phase-shifted pwm or level-shifted pwm?" in *2016 IEEE Energy Conversion Congress and Exposition (ECCE)*, Sep. 2016, pp. 1–7.

[9] J. Chavarria, D. Biel, F. Guinjoan, C. Meza, and J. J. Negroni, "Energy-balance control of pv cascaded multilevel grid-connected inverters under

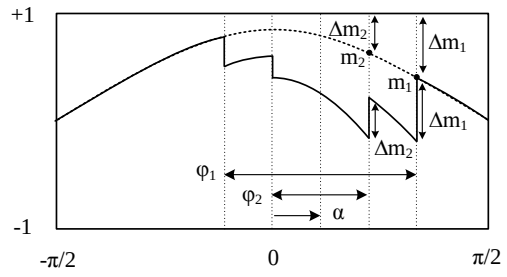

Fig. A-1: Non-clamped signal for strategy 3 when $\varphi_1 \geq \varphi_2$ to exemplify its constraint on maximum clamping angle.

level-shifted and phase-shifted pwms," *IEEE Transactions on Industrial Electronics*, vol. 60, no. 1, pp. 98–111, Jan 2013.

[10] M. Miranbeigi and H. Iman-Eini, "Hybrid modulation technique for grid-connected cascaded photovoltaic systems," *IEEE Transactions on Industrial Electronics*, vol. 63, no. 12, pp. 7843–7853, Dec 2016.

[11] B. Wu, *Cascaded H-Bridge Multilevel Inverters*. IEEE, 2006. [Online]. Available: https://ieeexplore.ieee.org/document/5238047

[12] S. Kouro, B. Wu, A. Moya, E. Villanueva, P. Correa, and J. Rodriguez, "Control of a cascaded h-bridge multilevel converter for grid connection of photovoltaic systems," in *2009 35th Annual Conference of IEEE Industrial Electronics*, Nov 2009, pp. 3976–3982.

[13] A. Dell'Aquila, M. Liserre, V. G. Monopoli, and P. Rotondo, "Overview of pi-based solutions for the control of dc buses of a single-phase h-bridge multilevel active rectifier," *IEEE Transactions on Industry Applications*, vol. 44, no. 3, pp. 857–866, May 2008.

[14] P. Guerriero, M. Coppola, F. Di Napoli, G. Brando, A. Dannier, D. Iannuzzi, and S. Daliento, "Three-phase pv chb inverter for a distributed power generation system," *Applied Sciences*, vol. 6, no. 10, October 2016.

[15] W. Mao, X. Zhang, Y. Hu, T. Zhao, F. Wang, F. Li, and R. Cao, "A research on cascaded h-bridge module level photovoltaic inverter based on a switching modulation strategy," *Energies*, vol. 12, May 2019.

[16] M. Coppola, F. Di Napoli, P. Guerriero, D. Iannuzzi, S. Daliento, and A. Del Pizzo, "An fpga-based advanced control strategy of a grid-tied pv chb inverter," *IEEE Transactions on Power Electronics*, vol. 31, no. 1, pp. 806–816, Jan 2016.

[17] W. Mao, X. Zhang, T. Zhao, Y. Hu, F. Wang, Z. Dai, and R. Cao, "Research on power equalization of three-phase cascaded h-bridge photovoltaic inverter based on the combination of hybrid modulation strategy and zero-sequence injection methods," *IEEE Transactions on Industrial Electronics*, pp. 1–1, 2019.

[18] X. Zhang, Y. Hu, W. Mao, T. Zhao, M. Wang, F. Liu, and R. Cao, "A grid-supporting strategy for cascaded h-bridge pv converter using vsg algorithm with modular active power reserve," *IEEE Transactions on Industrial Electronics*, pp. 1–1, 2020.

[19] L. Liu, H. Li, Y. Xue, and W. Liu, "Reactive power compensation and optimization strategy for grid-interactive cascaded photovoltaic systems," *IEEE Transactions on Power Electronics*, vol. 30, no. 1, pp. 188–202, Jan 2015.

[20] C. Wang, K. Zhang, J. Xiong, Y. Xue, and W. Liu, "A coordinated compensation strategy for module mismatch of chb-pv systems based on improved ls-pwm and reactive power injection," *IEEE Transactions on Industrial Electronics*, vol. 66, no. 4, pp. 2825–2836, April 2019.

[21] Y. Ko, V. Raveendran, M. Andresen, and M. Liserre, "Thermally-compensated discontinuous modulation for mvac/lvdc building blocks of modular smart transformers," *IEEE Transactions on Power Electronics*, pp. 1–1, 2019.

[22] J. I. Leon, S. Vazquez, and L. G. Franquelo, "Multilevel converters: Control and modulation techniques for their operation and industrial applications," *Proceedings of the IEEE*, vol. 105, no. 11, pp. 2066–2081, 2017.

[23] A. Marquez, J. I. Leon, V. G. Monopoli, S. Vazquez, M. Liserre, and L. G. Franquelo, "Generalized harmonic control for chb converters with unbalanced cells operation," *IEEE Transactions on Industrial Electronics*, vol. 67, no. 11, pp. 9039–9047, 2020.

[24] A. Marquez Alcaide, V. G. Monopoli, A. Tcai, J. I. Leon, G. Buticchi, S. Vazquez, M. Liserre, and L. G. Franquelo, "Discontinuous-pwm method for multilevel n-cell cascaded h-bridge converters," *IEEE Transactions on Industrial Electronics*, pp. 1–1, 2020.

[25] H. Iman-Eini, S. Bacha, and D. Frey, "Improved control algorithm for grid-connected cascaded h-bridge photovoltaic inverters under asymmetric operating conditions," *IET Power Electronics*, vol. 11, no. 3, pp. 407–415, 2018.

[26] H. Akagi, S. Inoue, and T. Yoshii, "Control and performance of a transformerless cascade pwm statcom with star configuration," *IEEE Transactions on Industry Applications*, vol. 43, no. 4, pp. 1041–1049, July 2007.

[27] A. M. Hava, R. J. Kerkman, and T. A. Lipo, "A high-performance generalized discontinuous pwm algorithm," *IEEE Transactions on Industry Applications*, vol. 34, no. 5, pp. 1059–1071, Sep. 1998.

[28] E. Demirok, P. C. Gonzalez, K. H. B. Frederiksen, D. Sera, P. Rodriguez, and R. Teodorescu, "Local reactive power control methods for overvoltage prevention of distributed solar inverters in low-voltage grids," *IEEE Journal of Photovoltaics*, vol. 1, no. 2, pp. 174–182, Oct 2011.

[29] N. R. Ullah, T. Thiringer, and D. Karlsson, "Voltage and transient stability support by wind farms complying with the e.on netz grid code," *IEEE Transactions on Power Systems*, vol. 22, no. 4, pp. 1647–1656, Nov 2007.

[30] Y. Ko, V. Raveendran, M. Andresen, and M. Liserre, "Advanced discontinuous modulation for thermally compensated modular smart transformers," *IEEE Transactions on Power Electronics*, vol. 35, no. 3, pp. 2445–2457, 2020.

[31] Y. Ko, M. Andresen, G. Buticchi, and M. Liserre, "Thermally compensated discontinuous modulation strategy for cascaded h-bridge converters," *IEEE Transactions on Power Electronics*, vol. 33, no. 3, pp. 2704–2713, March 2018.

[32] S. M. Sharkh, M. A. Abu-Sara, G. I. Orfanoudakis, and B. Hussain, *Loss Comparison of Two- and Three-Level Inverter Topologies*. IEEE, 2014. [Online]. Available: https://ieeexplore.ieee.org/document/6817729

[33] M. Liserre, V. G. Monopoli, A. Dell'Aquila, A. Pigazo, and V. Moreno, "Multilevel phase-shifting carrier pwm technique in case of non-equal dc-link voltages," in *IECON 2006 - 32nd Annual Conference on IEEE Industrial Electronics*, Nov 2006, pp. 1639–1642.

[34] A. Marquez, J. I. Leon, S. Vazquez, R. Portillo, L. G. Franquelo, E. Freire, and S. Kouro, "Variable-angle phase-shifted pwm for multilevel three-cell cascaded h-bridge converters," *IEEE Transactions on Industrial Electronics*, vol. 64, no. 5, pp. 3619–3628, May 2017.

[35] A. Marquez Alcaide, V. G. Monopoli, J. I. Leon, Y. Ko, G. Buticchi, S. Vazquez, M. Liserre, and L. G. G. Franquelo, "Sampling-time harmonic control for cascaded h-bridge converters with thermal control," *IEEE Transactions on Industrial Electronics*, pp. 1–1, 2019.

[36] K. Wang, M. Andresen, Y. Ko, and M. Liserre, "Cascaded multilevel topology based on quadruple active bridges for phase power balancing in large-scale pv systems," in *2019 21st European Conference on Power Electronics and Applications (EPE '19 ECCE Europe)*, 2019, pp. P.1–P.8.

Youngjong Ko (S'16-M'19) received the B.Sc and M.Sc degree in Electronic Engineering from the Ajou University, Suwon, South Korea in 2009 and 2012, respectively, and the Ph.D degree in 2019 from the chair of power electronics at the Christian-Albrechts-University of Kiel, Germany. He was a researcher in the LG Chem, Daejeon, South Korea from 2019 to 2020. From 2020, he is Assistant Professor in the department of electrical engineering at Pukyong National University, Busan, South Korea. His research interests include control and modulation of power converters and reliability in power electronics.

Markus Andresen (S'15-M'17) received the M.Sc.degree in electrical engineering and business administration in 2012 and the Ph.D degree in 2017 from the chair of power electronics at Christian-Albrechts-Unversity of Kiel, Germany. In 2010, he was an intern in the Delta Shanghai Design Centerat Delta Electronics (Shanghai) Co., Ltd., China and in 2017 he was a visiting scholar at the University of Wisconsin-Madison, USA. His current research interests include control of power converters and reliability in power electronics. Dr. Andresen was receipt of one IEEE price paper award on active thermal control of power electronics.

Kangan Wang received the B.S. degree and Ph.D. degree in Electrical Engineering from China University of Mining and Technology, China. From 2017 to 2019, He was a visiting Ph.D. student in the chair of power electronics, Department of Electrical and Electronic Engineering, Kiel University, Kiel, Germany. From 2020, he has been with Logistics Engineering College, Shanghai Maritime University. His research interests include power electronic-based smart transformer, cascaded H-bridge converter and dc-dc converter.

Marco Liserre (S'00-M'02-SM'07-F'13) received the M.S. and PhD degree in Electrical Engineering from the Bari Polytechnic, respectively in 1998 and 2002. He has been Associate Professor at Bari Polytechnic and from 2012 Professor in reliable power electronics at Aalborg University (Denmark). From 2013 he is Full Professor and he holds the Chair of Power Electronics at Kiel University (Germany), where he leads a team of more than 20 researchers with an annual budget of 2 Mill. Euro and cooperation with 20 companies. He has published over 350 technical papers (more than 110 of them in international peer-reviewed journals) and a book. These works have received more than 25000 citations. Marco Liserre is listed in ISI Thomson report "The world's most influential scientific minds" from 2014.

He has been awarded with an ERC Consolidator Grant for the project "The Highly Efficient And Reliable smart Transformer (HEART), a new Heart for the Electric Distribution System" and with the ERC Proof of Concept Grant U-HEART.

He is member of IAS, PELS, PES and IES. He has been serving all these societies in different capacities. He has received the IES 2009 Early Career Award, the IES 2011 Anthony J. Hornfeck Service Award, the 2014 Dr. Bimal Bose Energy Systems Award, the 2011 Industrial Electronics Magazine best paper award the Third Prize paper award by the Industrial Power Converter Committee at ECCE 2012, 2012, the 2017 IEEE PELS Sustainable Energy Systems Technical Achievement Award and the 2018 IEEE IES Mittelmann Achievement Award which is the highest award of the IEEE-IES.